nature cell biology

Caenorhabditis elegans EFA-6 limits microtubule growth at the cell cortex

Sean M. O'Rourke[1,2], Sara N. Christensen[1] and Bruce Bowerman[1,2].

Microtubules are polymers of tubulin heterodimers that exhibit dynamic instability: periods of growth followed by periods of shrinkage[1]. However, the molecular regulation of dynamic instability remains elusive. Here, we show that EFA-6, a cortically-localized protein[2], limits the growth of microtubules near the cell cortex of early embryonic cells from *Caenorhabidits elegans*, possibly by inducing microtubule catastrophes. Compared with wild type, embryos lacking EFA-6 had abnormally long and dense microtubules at the cell cortex, and growing microtubule plus ends resided at the cortex for up to five-fold longer. Loss of EFA-6 also caused excess centrosome separation and displacement towards the cell cortex early in mitosis, and subsequently a loss of anaphase spindle-pole oscillations and increased rates of spindle elongation. The centrosome separation phenotype was dependent on the motor protein dynein, suggesting a possible link between the modulation of microtubule dynamics at the cortex and dynein-dependent force production. EFA-6 orthologues activate ARF6-type GTPases to regulate vesicle trafficking[3]. However, we show that only the *C. elegans* EFA-6 amino-terminus is both necessary and sufficient to limit microtubule growth along the cortex, and that this function is independent of ARF-6.

During mitosis in one-cell stage *C. elegans* embryos, microtubule contact with the cell cortex is important for spindle positioning and function[4–8]. Microtubules are regulated so that their plus ends grow from centrosomes towards the cell cortex and reside there briefly before undergoing catastrophe and shrinkage through plus-end depolymerization, as in other systems[1,4,9]. Furthermore, the minus-end-directed microtubule-motor cytoplasmic dynein (hereafter designated as dynein) is thought to capture and pull on microtubule plus ends at the cortex to influence spindle position and function[10,11]. To identify genes that regulate dynein or influence microtubule dynamics, we previously identified 12 nonessential and conserved *C. elegans* loci that, when reduced in function, specifically suppress the lethality associated with conditional dynein heavy chain (*dhc-1*) mutations[2].

To investigate the requirements for these dynein suppressors, we depleted them and observed the first embryonic mitosis in live embryos. Depletion of one non-essential dynein suppressor, *efa-6*, resulted in several intriguing anomalies when we imaged the first cell cycle using time-lapse video microscopy (Fig. 1). In *control(RNAi)* embryos, sperm contributed paternal chromosomes and two centrosomes that remained attached to the male pronuclear envelope during pronuclear migration ($n = 25$; Fig. 1a). However, in *efa-6(RNAi)* embryos, one (38% of embryos) or both (38% of embryos) centrosomes detached from the male pronucleus and moved towards the cell cortex ($n = 24$; Fig. 1a and Supplementary Information, Fig. S1 and Movie S1). After the initial detachment, centrosomes always returned to the pronuclei in *efa-6(RNAi)* embryos with approximately normal separation, mitosis followed, and daughter cells displayed normal size asymmetry. There was a weak delay in pronuclear rotation: nuclear envelope breakdown occurred at 25 ± 14° ($n = 16$, range: 1–80°) in wild-type and at 40 ± 8° ($n = 22$, range: 5–81°) in *efa-6(tm3124)* embryos, but spindles always aligned along the anterior–posterior axis before anaphase in both strains. In embryos with reduced dynein function, centrosomes fail to separate or collapse towards each other before nuclear envelope breakdown[12,13]. After depleting *efa-6* in *dhc-1(or195*ts*)* embryos, centrosomes detached from the sperm pronucleus and centrosome separation was rescued at pronuclear meeting (Fig. 1a, b and Supplementary Information, Movie S2). However, *dhc-1(or195*ts*)* is not a null allele and still possesses some activity[13,14]. Thus, we used RNAi to more severely deplete *dhc-1*. In *dhc-1(RNAi)*; *efa-6(RNAi)* embryos there were multiple maternal pronuclei, unseparated centrosomes and no pronuclear migration. In these embryos, centrosomes never detached from the male pronucleus, indicating that dynein is required for the detachment observed in *efa-6(RNAi)* embryos (Fig. 1a and Supplementary Information, Movie S3). To test if microtubules are also required for the forces that pull centrosomes off the male pronucleus, we used a fast-acting temperature-sensitive dominant α-tubulin mutant, *tba-1(or346*dm,ts*)*, to partially disrupt microtubules in *efa-6*-depleted embryos[15]. This mutant expresses a TBA-1 protein with a single amino acid substitution (S377F) that could alter microtubule assembly, stability or interfere with microtubule-binding proteins, but in contrast to depleting α-tubulin with RNAi, robust asters are still present[15]. The

[1]Institute of Molecular Biology, 1229 University of Oregon, Eugene, Oregon 97403, USA.
[2]Correspondence should be addressed to S.M.O. or B.B. (e-mail: seanor@molbio.uoregon.edu and bbowerman@molbio.uoregon.edu)

Received 20 April 2010; accepted 18 October 2010; published online 14 November 2010; DOI: 10.1038/ncb2128

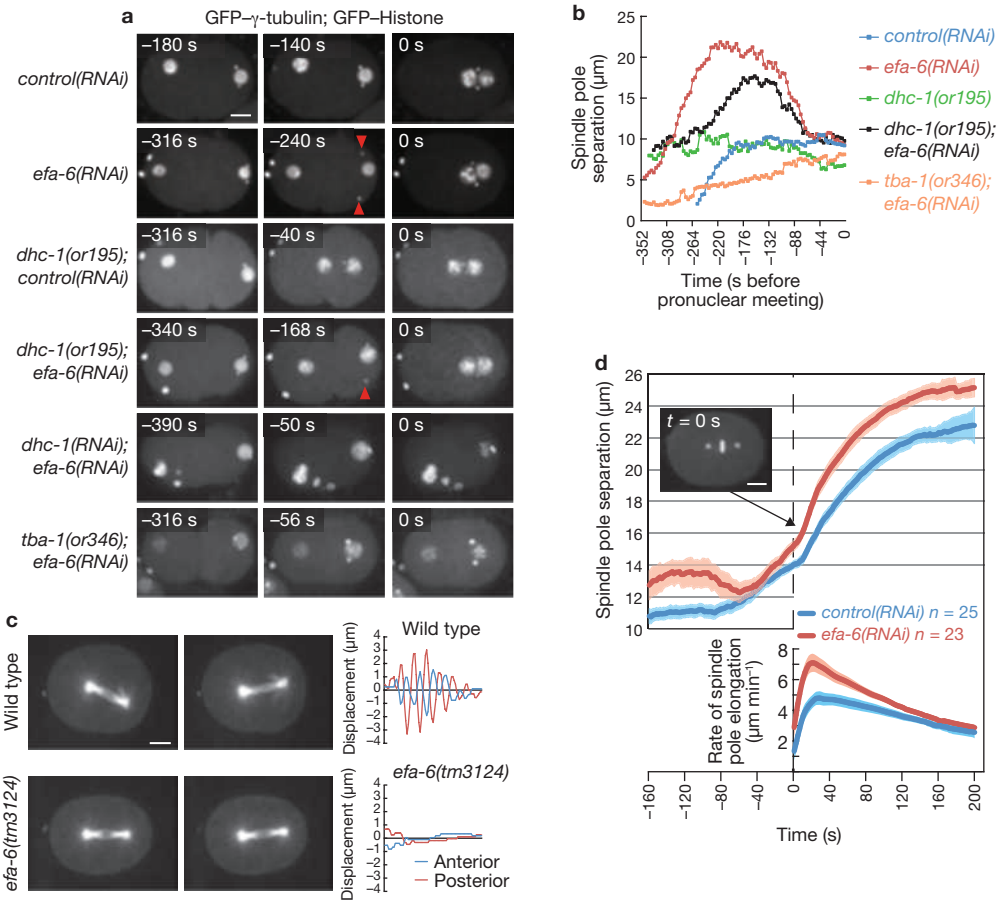

Figure 1 Loss of EFA-6 affects early microtubule-dependent processes. (**a**) Images from one-cell embryos expressing GFP–γ-tubulin and GFP–histone reporter fusions to mark centrosomes and chromosomes, respectively. Times indicated are relative to pronuclear meeting, or to paternal pronuclear envelope breakdown in the *dhc-1(RNAi); efa-6(RNAi)* and *tba-1(or346*dm,ts*); efa-6(RNAi)* embryos in which pronuclei did not meet. Multiple *z* sections were captured every 4–10 s and merged to give the images. Red arrowheads indicate localization of centrosomes that have detached from the male pronucleus. (**b**) Intercentrosomal distance over time during pronuclear migration for representative embryos. Spindle poles were tracked in three dimensions over time and the intercentrosomal distances were plotted. *dhc-1(or195*ts*)* and *tba-1(or346*dm,ts*)* mutant embryos were imaged for 30–120 min after shifting worms from 15 °C to 26 °C. The wild-type and *dhc-1(or195*ts*)* strains were grown on control RNAi-expressing bacteria. (**c**) Images (left) and plots of spindle pole transverse positions (right) of GFP–β-tubulin-expressing embryos. Left: three *z* sections 1 μm apart were captured every 2 s and merged. The two images of each embryo represent the extreme transverse distances travelled by the spindle poles during one oscillation. Right: spindle pole transverse positions were determined every 2 s for 152 s during anaphase. The *x* axes represent time. (**d**) Distances between spindle poles were plotted over the course of 6 min, starting before anaphase onset (corresponding to nuclear–centrosomal rotation and nuclear envelope breakdown) in a strain expressing GFP–γ-tubulin and GFP–histone. Each of the *efa-6(RNAi)* embryos had normal centrosome attachment to the pronuclei by this time. The time series were aligned at anaphase onset (dashed line). Images were captured every 2 s. The bottom plot indicates the rate of spindle elongation with respect to time. Data are means and the shaded regions represent the s.e.m. with a confidence interval of 0.95. Scale bars, 10 μm.

tubulin mutation completely blocked centrosome detachment, even though centrosome separation occurred (Figs 1a, b and Supplementary Information, Fig. S1). We conclude that both dynein and microtubules are required for the centrosome detachment and excess separation that occurs in the absence of *efa-6*.

Loss of *efa-6* function also caused two defects during anaphase. First, whereas *control(RNAi)* embryos always displayed robust spindle-pole oscillations, or spindle rocking, oscillations were greatly reduced in *efa-6(RNAi)* embryos, and the spindle-pole movements that did occur were aperiodic (Fig. 1c and Supplementary Information, Movie S4). Second, we found that the maximum anaphase spindle-pole separation rate was 48% faster in *efa-6*(*RNAi*) embryos (*control(RNAi)*, 4.80 ± 0.54 μm min^{-1}; *efa-6(RNAi)*: 7.10 ± 0.60 μm min^{-1}), and resulted in longer anaphase spindles, compared with *control*(*RNAi*) embryos (Fig. 1d).

As centrosome pronuclear detachment in *efa-6* mutants required functional microtubules, we used a β-tubulin fusion to green fluorescent protein (GFP) to image microtubules in live wild-type and *efa-6* mutant embryos. Wild-type one-cell stage embryos displayed very few long microtubules at the cell cortex, as reported previously[4]. However, we observed a dense network of abnormally long microtubules at the cell cortex in *efa-6* mutants (Fig. 2a and Supplementary Information, Movie S5). The increase was most pronounced during pronuclear migration (S Phase). Similarly to wild-type embryos[16], *efa-6(tm3124)* embryos exhibited cell-cycle-dependent changes in the density of microtubules, with the number of cortical microtubules substantially reduced during nuclear envelope breakdown, metaphase and anaphase. However, at each stage, microtubules were more abundant in *efa-6* embryos, compared with wild type (Supplementary Information, Fig. S2a).

The *efa-6(tm3124)* mutation is a deletion allele whereby the carboxy-terminal 456 amino acids of the Y55D9A.1.a EFA-6 isoform are replaced with 15 amino acids. *efa-6(tm3124), efa-6(RNAi),* and *efa-6(RNAi); efa-6(tm3124)* embryos each displayed indistinguishable microtubule phenotypes (data not shown). We next examined the length of the cortical microtubules in *efa-6*(–) and wild-type embryos. As microtubules were too dense to easily analyse at earlier stages, lengths were compared at pronuclear centration. Microtubules were almost 6-fold longer in *efa-6(RNAi)* embryos when compared with wild type (Fig. 2b). A greater abundance of cortical interphase microtubules were observed again in two-cell stage embryos, with the mutants displaying substantially longer and denser cortical microtubules (Fig. 2a, middle row). Interestingly, in four-cell or later stage embryos, dense cortical microtubules were present in both mutant and wild-type blastomeres (Fig. 2a, bottom row; Supplementary Information, Fig. S2b). We have previously shown that EFA-6 is enriched at the anterior cortex in one and two-cell embryos, but is absent in blastomeres of later stage embryos[2]. We measured the levels across the embryo cortex and found that GFP–EFA-6 is present throughout the cortex, but at reduced levels in the posterior (Supplementary Information, Fig. S3). We conclude that EFA-6 is present and functions in one- and two-cell stage embryos, but not in later stage embryos, to limit the extent of microtubule growth throughout the cell cortex.

To quantify how EFA-6 influences microtubule dynamics, we used a GFP fusion to EBP-2, a conserved protein that binds specifically to growing microtubule plus ends, to measure microtubule growth, polymerization rates and plus-end cortical-residency times[9]. In wild-type embryos, EBP-2–GFP foci resided at the cortex for brief periods before the microtubules underwent catastrophe or pausing (1.3 ± 0.11 s, mean ± s.e.m.; range: 0.25–2.25 s, n = 63; Fig. 3 and Supplementary Information, Movie S6; these data are consistent with previous studies[4,9]). However, in *efa-6* mutant embryos individual EBP-2 foci remained associated with and tracked along the cortex for much longer times (5.1 ± 0.35 s, mean ± s.e.m.; range: 1.25–9.75 s, n = 117; Fig. 3 and Supplementary Information, Movie S6). There was also an increased number of plus ends at the cortex in *efa-6* mutant embryos (wild type and *efa-6(tm3124)*; 0.036 ± 0.004 and 0.101 ± 0.009 EBP-2 foci μm^{-2}, respectively; means ± s.e.m.), consistent with the increased residency time for plus ends and growth along the cortex. Importantly, EFA-6 activity was limited to the cortex, because astral microtubule nucleation rates and cytoplasmic microtubule growth rates were similar in *efa-6*(–) mutant and wild-type embryos (Fig. 3d). We conclude that EFA-6 limits microtubule plus-end residency time at the cortex, but does not regulate the microtubule nucleation or polymerization rates of astral microtubules. Thus, EFA-6 could either promote microtubule catastrophe, or pausing of plus-end growth[17,18], at the cell cortex.

Cortically localized dynein is thought to pull on microtubule plus ends to influence mitotic spindle assembly and spindle position in one-cell-stage embryos[8,10–12,19], and embryos with reduced dynein activity lack spindle oscillations[10,13]. As we had identified *efa-6* as a dynein suppressor, the possibility that EFA-6 regulates dynein localization at the cell cortex was tested. We found that a GFP–DHC-1 fusion protein[20] was localized to puncta at the cell cortex of one-cell stage embryos, similarly to EBP-2 puncta (Supplementary Information, Fig. S4a and Movie S7). However, persistence of DHC-1 foci at the cortex did not depend on EFA-6 (Supplementary Information, Fig. S4b and c). We also assayed

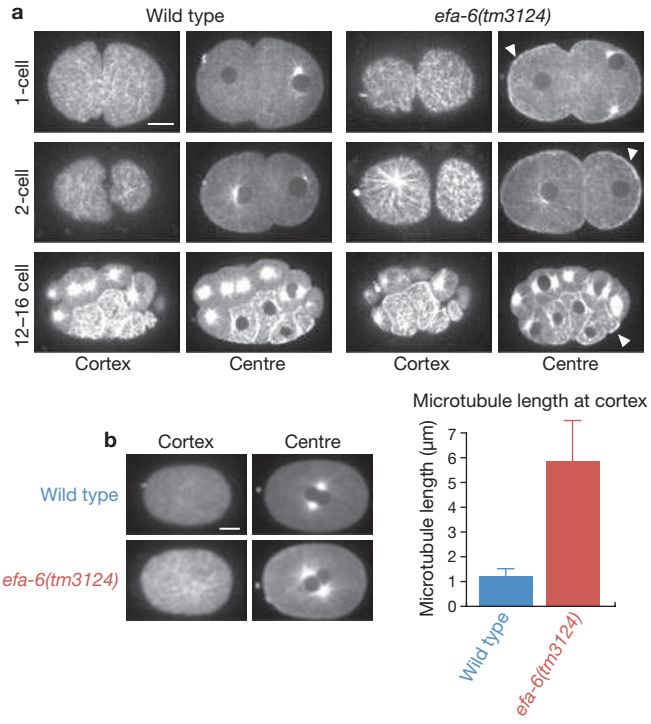

Figure 2 EFA-6 prevents long cortical microtubules in one- and two-cell embryos. (**a**) Images from wild-type and *efa-6(tm3124)* embryos expressing GFP–β-tubulin. Three *z* sections with 0.5 μm spacing were captured and merged to generate the images. Shown for each time point are images captured at the cortical focal plane (left) and the central focal plane (right). Top row: one-cell-stage embryos, middle row: two-cell-stage embryos, Bottom row: 12–16-cell-stage embryos. Arrowheads indicate examples of enhanced cortical GFP–β-tubulin in central focal planes. (**b**) Left: representative images of wild-type and *efa-6(tm3124)* embryos, expressing GFP–β-tubulin, at the cortical focal plane (left) and central focal plane (right). Right: cortical microtubule lengths were determined 100–105 s after pronuclear meeting; 107 microtubules were measured from 9 embryos for the wild type, and 118 microtubules were measured from 10 embryos for *efa-6(tm3124)*. Data are means ± s.e.m. with a confidence interval of 0.95. Scale bars, 10 μm.

cortical microtubules in embryos depleted for *dhc-1*, or both *dhc-1* and *efa-6*, to determine if dynein is required for the dense microtubule phenotype in *efa-6*(–) embryos. Cortical microtubules seemed normal after reducing *dhc-1* activity, but they were still long and abundant when *dhc-1* and *efa-6* were co-depleted (Supplementary Information, Fig. S5). We conclude that EFA-6 does not regulate microtubule dynamics by influencing cortical dynein localization, and that dynein is not required for the long cortical microtubules in *efa-6*(–) embryos.

To determine which portions of EFA-6 limit cortical microtubule growth, we made and expressed a series of EFA-6 mutant constructs. The *efa-6* gene encodes a potential guanine nucleotide exchange factor for ARF6-type small G proteins. It contains a sec7 GDP–GTP exchange domain, a pleckstrin homology (PH) domain, and a predicted coiled-coil region. We constructed a point mutation in a conserved catalytic residue that when mutated in other systems abolishes exchange factor activity, and deletion alleles that individually lacked the sec7, PH, coiled-coil domains, and the N-terminal and C-terminal regions. We expressed GFP alone (as negative control) or these mutant *efa-6* constructs in *efa-6(tm3124)* mutant worms. GFP-alone control embryos had cytoplasmic fluorescence and spindle oscillations were

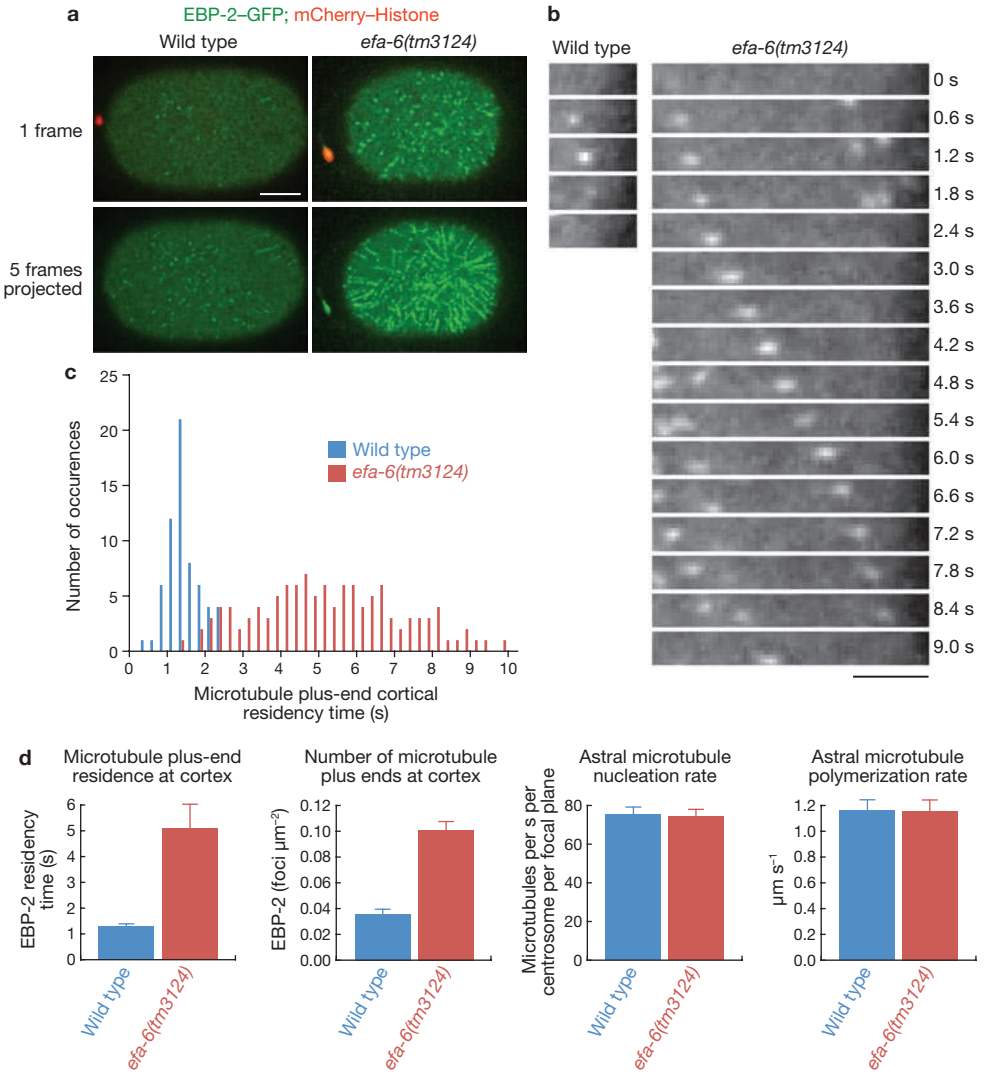

Figure 3 EFA-6 limits microtubule growth at the cortex. (**a**) Images of embryos, expressing EBP2–GFP and mCherry–histone, at the cortical focal plane after pronuclear meeting. Top, single-frame images; bottom, images merged from five frames, captured at 1 s intervals. At the cortical plane, wild-type embryos have EBP-2–GFP puncta that tracked for short times as seen in the merged time points. Embryos lacking EFA-6 demonstrated EBP-2–GFP puncta tracking along the cortex for extended periods, which resulted in lines of puncta in the projected image. See Supplementary Information, Movie S6 for the entire time series. Scale bar, 10 μm. (**b**) Single cortical EBP-2–GFP puncta were tracked and imaged in wild-type and *efa-6(tm3124)* embryos. Each image shows the position of EBP-2–GFP puncta in an area of the cortex at the indicated times. Scale bar, 4 μm. (**c**) Residency time of EBP-2–GFP puncta at the cortex (number of plus ends; 63, wild-type, 117 *efa-6(tm3124)*). EBP-2–GFP puncta were tracked over time as shown in **c**. (**d**) Microtubule dynamics in wild-type and *efa-6(tm3124)* embryos. Dynamics were quantified by imaging embryos expressing the EBP-2–GFP reporter. Data are means ± s.e.m. with a confidence interval of 0.95. Microtubule plus-end residence at the cortex, astral microtubule nucleation rate, and the astral microtubule polymerization rate were determined at pronuclear meeting, the numbers of microtubule plus ends at the cortex was determined 15 s after pronuclear meeting.

absent (Fig. 4a). The wild-type EFA-6 GFP fusion protein localized to the cortex and promoted robust spindle rocking, as did the catalytically inactive point mutant, the sec7 deletion mutant, the coiled-coil deletion mutant, and the C-terminal deletion mutant (Fig. 4a). Thus, it seems exchange factor activity is not important for microtubule regulation, and a small G-protein is probably not involved. The PH domain of the mammalian EFA6 mediates attachment to the cortex by interacting with phosphatidylinositol 4,5-bisphosphate lipids[21]. As expected, the PH domain mutant was exclusively cytoplasmic and spindle oscillations were absent, suggesting that membrane tethering is required for microtubule regulation. Finally, the N-terminal deletion mutant was localized to the cortex but spindle rocking was absent. We conclude that the PH domain and the N-terminus, but not GTPase activity, are required for spindle oscillations.

Chimaeric protein fusions were used to further elucidate requirements for the EFA-6 N-terminus. To test whether the *C. elegans* EFA-6 N-terminal region can regulate microtubule dynamics independently of other EFA-6 sequences so long as it is cortically localized, we expressed the EFA-6 N-terminus fused to the *C. elegans* MIG-2 CAAX box to link it to the plasma membrane independently of its endogenous PH domain[22,23]. GFP–EFA-6$^{N\text{–terminus+CAAX}}$ was membrane-localized and promoted spindle oscillations in *efa-6*(–) embryos, but the control GFP–EFA-6$^{N\text{–terminus+SAAX}}$ protein was cytoplasmic and did not promote rocking (Fig. 4a). Thus, the EFA-6 N-terminal region regulates spindle function

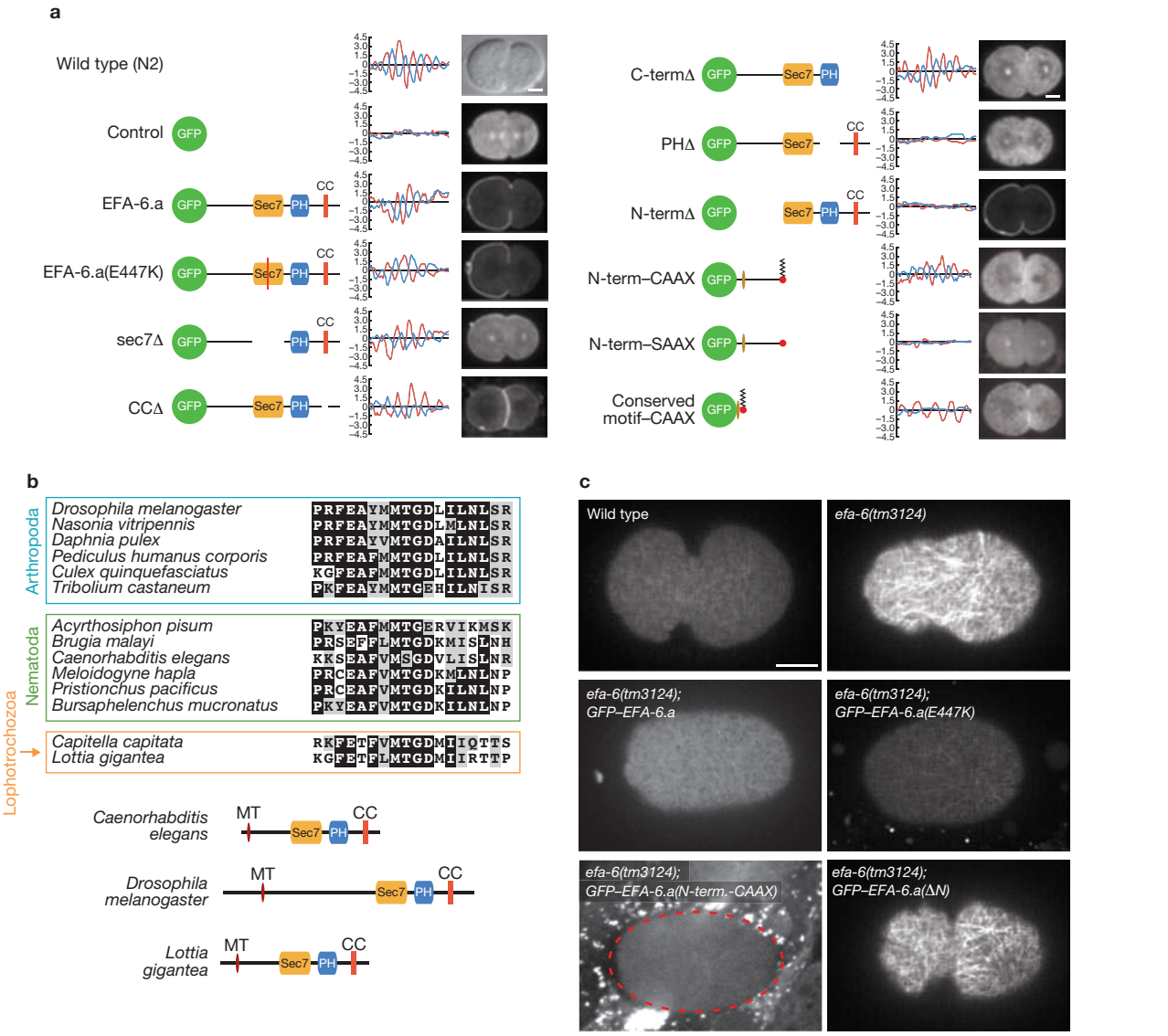

Figure 4 Determination of the EFA-6 microtubule-regulating residues. (**a**) Effect of EFA-6 domain deletion on spindle oscillations. Left: schematic representations of the indicated EFA-6 constructs. EFA-6.a; wild-type EFA-6 fused to GFP, and the construct used to make the mutants and other constructs. EFA-6.a(E447K); Glu 447 of EFA-6 substituted with a lysine residue. sec7Δ, CCΔ, C-termΔ, PHΔ and N-termΔ; deletion of the indicated domains, residues 684–816 (C-termΔ) or residues 2–352 (N-termΔ) from EFA-6. N-term–CAAX; amino-acid residues 1–353 of EFA-6 fused to the CAAX peptide. N-term–SAAX; amino-acid residues 1–353 of EFA-6 fused to SAAX, a mutant CAAX domain. Conserved motif–CAAX; a start codon and amino-acid residues 26–60 of EFA-6 fused to CAAX. Plasmids encoding GFP or the constructs were transformed into *efa-6(tm3124)* mutant worms. Middle: spindle pole transverse positions were determined every 1 s for 152 s during anaphase. Right: fluorescence microscopy images of a representative embryo (mid-embryonic *z* section) demonstrating localization of the GFP-tagged proteins at telophase/cytokinesis (for the wild-type embryo, a DIC image is presented). (**b**) Top: alignment of the conserved EFA-6 N-terminal motif from several animal phyla and species. Bottom: schematic representation of the position of the domain in the context of the full-length proteins of the nematode *C. elegans*, the insect *Drosophila melanogaster* and the mollusk *Lottia gigantea*. (**c**) Images of mCherry–TBA-1-labelled cortical microtubules in one-cell embryos were obtained by merging three *z* sections (each section 0.5 μm apart). Dashed red line indicates the embryo boundary in the bottom left image. Scale bars, 10 μm.

independently of the other domains if it is at the cortex. Additionally, we assayed centrosome detachment from the male pronucleus in the GFP–EFA-$6^{N\text{–terminus+CAAX}}$ embryos and found that the fusion protein partially rescued the detachment phenotype (76% of the embryos had two attached centrosomes, 24% of the embryos had one detach, and no embryos had both detach, $n = 21$). We then identified an 18 amino acid conserved motif present in the N-terminus of EFA-6 proteins in nematodes, arthropods and lophotrochozoa (Fig. 4b). Other than this motif, the N-terminus of EFA-6 shows little sequence conservation among different phyla. A 45 amino-acid fragment containing this motif fused to GFP and the CAAX box was expressed in early embryos. This chimaeric protein was present at the cortex and promoted periodic spindle oscillations (Fig. 4a). Thus, this limited region is sufficient to regulate spindle function. Consistent with this deletion analysis, we did not find defects in centrosome–pronucleus attachment or spindle rocking in embryos depleted for *arf-6* (data not shown), which encodes the small GTPase that is regulated by the guanine nucleotide exchange activity of *efa-6* (ref. 3). We conclude that EFA-6 does not function through ARF-6 to regulate microtubule dynamics.

To determine if the different *efa-6* gene constructs rescued spindle rocking by reducing the abundance of microtubules at the cortex, we imaged cortical microtubules in a number of the strains. In *efa-6*(–) embryos, expression of wild-type EFA-6, the catalytic point mutant, and the EFA-6$^{N\text{–terminus+CAAX}}$ transgenes resulted in short cortical microtubules, whereas dense arrays of long cortical microtubules persisted after expression of the N-terminal deletion mutant (Fig. 4c). We conclude that the EFA-6 N-terminus, when cortically tethered, is both necessary and sufficient to limit cortical microtubule abundance. Although the EFA-6 N-terminus can inhibit cortical microtubules independent of its GTPase activity, it is intriguing that the conserved N-terminal motif we have identified is found only in EFA-6 orthologues. Thus, the linkage of the N-terminal and GTPase modules is widely conserved. It will be interesting to learn if either function can, in some circumstances, influence the other.

In summary, we have shown that EFA-6 is a cortical protein in the early *C. elegans* embryo that limits microtubule length, centrosome separation and spindle-elongation rates by altering microtubule dynamics at the cell cortex. EFA-6 could regulate the dynamics of microtubules in a number of ways. First, EFA-6 could promote microtubule plus-end catastrophe or pausing directly. Alternatively, EFA-6 could regulate a distinct factor that functions on the cortical microtubules. Finally, EFA-6 could either alter microtubule tip flexibility or the rigidity of the cell cortex as microtubules display enhanced catastrophe events when growing into a surface[24].

The long cortical microtubules that develop in *efa-6*(–) embryos seem to generate increased pulling forces on centrosomes, as they are associated with increased centrosome separation both during pronuclear migration and during mitotic anaphase. In contrast, reduced spindle oscillations are usually associated with decreased cortical forces[8,10]. Nevertheless, in *efa-6*(–) embryos either altered microtubule dynamics or increased microtubule length also seem to limit oscillations, perhaps through disruption of feedback regulation that is thought to promote spindle-pole rocking[4,8,10].

Dynein is hypothesised to be a cortical force generator that causes astral microtubules to pull on centrosomes in the early *C. elegans* embryo[8,10–12,19], and we have demonstrated that it is in fact present at the cortex in discreet foci that persist for time frames similar to microtubule plus ends (Supplementary Information, Fig. 4). Furthermore, we find that centrosomes do not travel from the male pronucleus toward the cortex in embryos depleted for both *dhc-1* and *efa-6* (Fig. 1 and Supplementary Information, Movie S3). Thus, dynein in *efa-6*(–) embryos seemed to be increased in activity, perhaps as a result of either the increased lateral microtubule–cortex interactions, or the longer residency time of microtubule plus ends at the cortex.

In a broader context, our findings illustrate the value of studying nonessential conserved genes to better understand essential biological processes. As in other model organisms, most cytoskeletal regulators in *C. elegans* have been identified in screens for essential genes. However, most eukaryotic genes are not essential. In budding yeast and *C. elegans*, in which extensive genome-wide screens have been performed, only 7–19% of protein-coding genes are required for viability[25–27]. Nevertheless, nonessential genes like *efa-6* can clearly have important roles in modulating essential processes[2,28–30]. Identifying functions for nonessential genes is important because many human disease gene orthologues are not essential in model organisms. For example, even in the mouse, 47% of human disease gene orthologues are not essential when assayed with null mutations[31]. □

METHODS

Methods and any associated references are available in the online version of the paper at http://www.nature.com/naturecellbiology/

Note: Supplementary Information is available on the Nature Cell Biology website

ACKNOWLEDGEMENTS

We thank M. Price, G. von Dassow, L. Pelletier, and C. Doe for insightful discussions; M. Goulding and E. Munro for technical advice; S. Schneider for advice on taxonomical and sequence alignments; S. Mitani for isolating and providing *efa-6(tm3124)*; V. Davis Haug for the mC-TBA-1 strain; and C. Doe and C. Cabernard for comments on the manuscript. S.M.O was supported by the Leukemia and Lymphoma Society of America, S.M.O. and B.B. are supported by NIH R01GM058017 and R01GMO49869.

AUTHOR CONTRIBUTIONS

S.M.O. and B.B. designed the experiments and wrote the paper. S.M.O. conceived the project, performed the experiments and analysed the data. Microscopy and strain generation were also contributed by S.N.C.

COMPETING FINANCIAL INTERESTS

The authors declare no competing financial interests.

Published online at http://www.nature.com/naturecellbiology
Reprints and permissions information is available online at http://npg.nature.com/reprintsandpermissions/

1. Mitchison, T. & Kirschner, M. Dynamic instability of microtubule growth. *Nature* **312,** 237–242 (1984).
2. O'Rourke, S. M., Dorfman, M. D., Carter, J. C. & Bowerman, B. Dynein modifiers in *C. elegans*: light chains suppress conditional heavy chain mutants. *PLoS Genet.* **3**, e128 (2007).
3. Franco, M. *et al.* EFA6, a sec7 domain-containing exchange factor for ARF6, coordinates membrane recycling and actin cytoskeleton organization. *EMBO J.* **18,** 1480–1491 (1999).
4. Kozlowski, C., Srayko, M. & Nedelec, F. Cortical microtubule contacts position the spindle in *C. elegans* embryos. *Cell* **129,** 499–510 (2007).
5. Siller, K. H. & Doe, C. Q. Spindle orientation during asymmetric cell division. *Nat. Cell Biol.* **11,** 365–374 (2009).
6. Oegema, K. & Hyman, A. A. Cell division. *WormBook*, 1–40 (2006).
7. Dumont, S. & Mitchison, T. J. Force and length in the mitotic spindle. *Curr. Biol.* **19,** R749–R761 (2009).
8. Grill, S. W., Howard, J., Schaffer, E., Stelzer, E. H. & Hyman, A. A. The distribution of active force generators controls mitotic spindle position. *Science* **301,** 518–521 (2003).
9. Srayko, M., Kaya, A., Stamford, J. & Hyman, A. A. Identification and characterization of factors required for microtubule growth and nucleation in the early *C. elegans* embryo. *Dev. Cell* **9,** 223–236 (2005).
10. Pecreaux, J. *et al.* Spindle oscillations during asymmetric cell division require a threshold number of active cortical force generators. *Curr. Biol.* **16,** 2111–2122 (2006).
11. Severson, A. F. & Bowerman, B. Myosin and the PAR proteins polarize microfilament-dependent forces that shape and position mitotic spindles in *Caenorhabditis elegans*. *J. Cell Biol.* **161,** 21–26 (2003).
12. Gönczy, P., Pichler, S., Kirkham, M. & Hyman, A. A. Cytoplasmic dynein is required for distinct aspects of MTOC positioning, including centrosome separation, in the one cell stage *Caenorhabditis elegans* embryo. *J. Cell Biol.* **147,** 135–150 (1999).
13. Schmidt, D. J., Rose, D. J., Saxton, W. M. & Strome, S. Functional analysis of cytoplasmic dynein heavy chain in *Caenorhabditis elegans* with fast-acting temperature-sensitive mutations. *Mol. Biol. Cell* **16,** 1200–1212 (2005).
14. Hamill, D. R., Severson, A. F., Carter, J. C. & Bowerman, B. Centrosome maturation and mitotic spindle assembly in *C. elegans* require SPD-5, a protein with multiple coiled-coil domains. *Dev. Cell* **3,** 673–684 (2002).
15. Phillips, J. B., Lyczak, R., Ellis, G. C. & Bowerman, B. Roles for two partially redundant alpha-tubulins during mitosis in early *Caenorhabditis elegans* embryos. *Cell Motil. Cytoskeleton* **58,** 112–126 (2004).
16. Hyman, A. A. & White, J. G. Determination of cell division axes in the early embryogenesis of *Caenorhabditis elegans*. *J. Cell Biol.* **105,** 2123–2135 (1987).
17. Sammak, P. J. & Borisy, G. G. Direct observation of microtubule dynamics in living cells. *Nature* **332,** 724–726 (1988).
18. Schulze, E. & Kirschner, M. New features of microtubule behaviour observed *in vivo*. *Nature* **334,** 356–359 (1988).
19. Skop, A. R. & White, J. G. The dynactin complex is required for cleavage plane specification in early *Caenorhabditis elegans* embryos. *Curr. Biol.* **8,** 1110–1116 (1998).

20. Gassmann, R. *et al.* A new mechanism controlling kinetochore-microtubule interactions revealed by comparison of two dynein-targeting components: SPDL-1 and the Rod/Zwilch/Zw10 complex. *Genes Dev.* **22,** 2385–2399 (2008).
21. Macia, E. *et al.* The pleckstrin homology domain of the Arf6-specific exchange factor EFA6 localizes to the plasma membrane by interacting with phosphatidylinositol 4, 5-bisphosphate and F-actin. *J. Biol. Chem.* **283,** 19836–19844 (2008).
22. Diogon, M. *et al.* The RhoGAP RGA-2 and LET-502/ROCK achieve a balance of actomyosin-dependent forces in *C. elegans* epidermis to control morphogenesis. *Development* **134,** 2469–2479 (2007).
23. Portereiko, M. F. & Mango, S. E. Early morphogenesis of the *Caenorhabditis elegans* pharynx. *Dev. Biol.* **233,** 482–494 (2001).
24. Janson, M. E., de Dood, M. E. & Dogterom, M. Dynamic instability of microtubules is regulated by force. *J. Cell Biol.* **161,** 1029–1034 (2003).
25. Giaever, G. *et al.* Functional profiling of the *Saccharomyces cerevisiae* genome. *Nature* **418,** 387–391 (2002).
26. Kamath, R. S. *et al.* Systematic functional analysis of the *Caenorhabditis elegans* genome using RNAi. *Nature* **421,** 231–237 (2003).
27. Sönnichsen, B. *et al.* Full-genome RNAi profiling of early embryogenesis in *Caenorhabditis elegans*. *Nature* **434,** 462–469 (2005).
28. Labbé, J. C., Pacquelet, A., Marty, T. & Gotta, M. A genome-wide screen for suppressors of *par-2* uncovers potential regulators of PAR protein-dependent cell polarity in *Caenorhabditis elegans*. *Genetics* **174,** 285–295 (2006).
29. Tong, A. H. *et al.* Systematic genetic analysis with ordered arrays of yeast deletion mutants. *Science* **294,** 2364–2368 (2001).
30. Dorfman, M., Gomes, J. E., O'Rourke, S. & Bowerman, B. Using RNA interference to identify specific modifiers of a temperature-sensitive, embryonic-lethal mutation in the *Caenorhabditis elegans* ubiquitin-like Nedd8 protein modification pathway E1-activating gene *rfl-1*. *Genetics* **182,** 1035–1049 (2009).
31. Park, D., Park, J., Park, S. G., Park, T. & Choi, S. S. Analysis of human disease genes in the context of gene essentiality. *Genomics* **92,** 414–418 (2008).

DOI: 10.1038/ncb2128

METHODS

***C. elegans* strains and culture.** Strains were maintained according to standard procedures[32]. Temperature-sensitive strains were maintained at 15 °C, non-temperature-sensitive strains were maintained at room temperature, except GFP–EFA-6-expressing strains, which were maintained at 25 °C. Strains expressing GFP–γ-tubulin and GFP–histone H2b- were derived from TH32 (ref. 33), GFP–β-tubulin-expressing strains were derived from WH204 (ref. 34), and mCherry–histone H2b-expressing strains were derived from OD57 (ref. 35). For transformation of *C. elegans*, we used the microparticle bombardment method[2,36].

RNAi. *Escherichia coli* clones expressing dsRNA to deplete *dhc-1* and *efa-6* were obtained from the MRC Geneservice (Cambridge, UK)[26,37]. The oligonucleotides used to produce the *dhc-1* construct had the sequence: 5′-AAGGAAGGAGCTCAACGACA-3′ and 5′-CCTTTCCTTCCTGGGTCTTC-3′, and the *efa-6* gene fragment was amplified with 5′-CCGTCTTGATGTTGAAGCAA-3′ and 5′-GGACACTCCGTCGAAACATT-3′; both used *C. elegans* genomic DNA as template[26,37]. We produced the *arf-6(RNAi)* clone by amplifying N2 genomic DNA with the following two oligonucleotides: 5′-AAGATATCGGAGCTCCGGATATTAATGCT-3′ and 5′-AAGATATCCCCAATTTATCCTGAATTTCGT-3′. After cleavage with *Eco*RV and ligation to *Eco*RV-cleaved L4440 vector, the plasmid was introduced into the HT115(DE3) RNAi feeding bacterial strain as described[37]. RNAi to reduce the function of *efa-6* was performed by placing L1 larvae synchronized by hypochlorite hatch-off onto 60-mm nematode growth medium (NGM)-agar plates with 100 mg ml^{-1} ampicillin and 1 mM isopropyl-β-D-thiogalactopyranoside, and seeded with the double-stranded RNA-expressing *E. coli*, as described[2]. For co-depletions, we transferred L4 larvae to plates seeded with an equal mixture of the double-strand RNA-expressing *E. coli* strains. We examined *dhc-1*-depleted embryos 27–37 h after the transfer and only analysed embryos that had multiple maternal pronuclei, unseparated centrosomes, and lacked pronuclear migration, indicating a strong dynein depletion.

Microscopy. Imaging of fluorescent fusion proteins was accomplished by mounting embryos on 3% (w/v) agar pads on microscope slides covered with a coverslip. Slides were analysed on a Leica DMI 4000B microscope fitted with a Leica ×63 1.40–0.60 HCX Plan Apo oil objective lens in a room maintained at 25 °C. Time-lapse microscopy videos were obtained with a Hammamatsu EM-CCD (electron-multiplying-charged-coupled device) digital camera using Volocity software (Perkin Elmer). After recording, the videos were adjusted for position and contrast in ImageJ (http://rsb.info.nih.gov/ij/). For images of GFP–β-tubulin-expressing embryos, we normalized the images such that the nuclear fluorescence in interphase cells was similar.

Analysis of spindle pole positions. We recorded spindle pole positions using the ImageJ package 'MTrackJ' (http://www.imagescience.org/meijering/). From these coordinates we calculated the distance between spindle poles. Measurements from multiple embryos were synchronized at anaphase onset to produce the graphs in Figure. 1d. To find the spindle pole separation rates for each time after anaphase onset, we divided the distance travelled (beginning at anaphase onset) by the time elapsed. The greatest rate for *control(RNAi)* embryos occurred 30 s after anaphase onset and the greatest rate for *efa-6(RNAi)* embryos occurred 22 s after anaphase onset. The errors given in the text represent the s.e.m. with a confidence interval of 0.95.

Quantification of microtubule and DHC-1 kinetics. To calculate microtubule nucleation rates, we followed a previously published procedure[9]. Briefly, a single focal plane was captured every 0.5 s for 1 min while focused on a centrosome beginning at pronuclear meeting. We then used the kymograph function in the ImageJ package 'TimeSpacePlot' (http://www.embl.de/eamnet/html/kymograph.html) to draw a semicircle at a distance of 9 μm from the centre of the centrosome and produced kymographs corresponding to the 1 min video micrograph. By counting the number of spots, we determined the number of microtubule plus ends passing the semicircle in one minute. We counted 602 microtubule plus ends from eight wild-type embryos and 521 microtubules from seven *efa-6(tm3124)* embryos.

We determined the number of EBP-2–GFP and GFP–DHC-1 puncta at the cortex by analysing an image of the cortex 15 s after pronuclear meeting in the transgene-expressing embryos. We drew a rectangle that included only cortical regions of the embryo (because the amount of cortical area visible varied in each embryo) and counted the number of puncta present and the area of the rectangle in ImageJ. The rectangle was positioned such that both anterior and posterior regions were equally sampled. We then calculated the number of puncta per μm^2 of cortex.

To quantify microtubule plus end and GFP–DHC-1 cortical residency times, we performed time-lapse microscopy on the cortex of EBP-2–GFP- or GFP–DHC-1-expressing embryos. Images were acquired for 30 s, beginning at pronuclear meeting, at a rate of 4 images per s (for EBP-2–GFP-expressing embryos) or 3 frames per s (for GFP–DHC-1-expressing embryos). At least five embryos were analysed for determining each measurement. The images were then analysed in ImageJ with the measurement tool. As GFP puncta appeared we counted how many frames they each persisted, giving residency times. For determining the GFP–DHC-1 residency times, we first filtered the images with a Laplacian filter using the default parameters in the ImageJ package 'FeatureJ' (http://www.imagescience.org/meijering/).

Determination of astral microtubule polymerization rates was performed as previously reported[9]. We tracked individual EBP-2–GFP puncta, from pronuclear meeting that began at a centrosome to when they moved towards the cell cortex, using the ImageJ package 'MTrackJ' (http://www.imagescience.org/meijering/). Dividing the total distance travelled by the number of frames (time) yielded the rate of polymerization. The microtubule polymerization rate was 1.2 ± 0.09 μm s^{-1} for both wild type and *efa-6(tm3124)* embryos. We tracked 83 microtubules from six wild-type embryos and 65 microtubules from five *efa-6(tm3124)* embryos.

We assayed pronuclear–centrosomal complex rotation by measuring the angles of the two centrosomes relative to the anterior–posterior axis in wild-type or *efa-6(tm3124)* embryos expressing GFP–β-tubulin. The angles were determined when cytoplasmic GFP–β-tubulin began to enter the nuclei, indicating nuclear envelope breakdown.

Molecular Biology. For constructing the *efa-6* variants, we started with a cDNA clone for *Y55D9A.1.a* (encoding EFA-6.a) isolated previously and contained in the pGEM-T easy vector (Promega)[2]. The glutamic acid codon at amino acid position 447 in EFA-6.a was changed to a lysine codon by using the QuikChange II Site-Directed Mutagenesis Kit (Agilent Technologies). After sequencing of the product to detect successful mutagenesis, the cDNA was sub cloned into the pSO26 vector using *Sgf*I (Promega) and *Spe*I (New England Biolabs) restriction enzymes. pSO26 contains the maternal *pie-1* promoter to express cDNA clones as well as an *unc-119*(+) gene for selecting *C. elegans* transformants[2]. Similarly, we used the QuikChange method to produce the sec7, pleckstrin homology, coiled-coil, C-terminal, and N-terminal deletion mutants in the *Y55D9A.1.a* cDNA. For expressing the N-terminal fragments with either the CAAX or SAAX box, we amplified the *Y55D9A.1.a* cDNA with oligonucleotides which included sequence encoding the additional protein tag and cloned them into pSO26, as previously described[22,23]. The sec7 domain mutant deleted amino acids 354–530, the pleckstrin homology domain mutant deleted amino acids 567–683, the coiled-coil deletion removed amino acids 711–736, the C-terminal deletion mutant lacked amino acids 684–816, and the N-terminal deletion mutant lacked amino acids 2–352 of EFA-6. The N-terminus (containing amino acids 1–353 of EFA-6) was fused to the MIG-2 CAAX box peptide (KPQKKKKSCNIM) or to a mutant version, 'SAAX' (KPQKKKKSSNIM). Finally, the conserved motif construct present in the N-terminus contained a start codon and amino acids 26–60, followed by the MIG-2 CAAX box. The *efa-6* plasmids were then transformed into *unc-119(ed3); efa-6(tm3124)* mutant worms. At least 10 DIC (differential interference contrast) microscopy images were recorded for each construct to monitor spindle oscillations; one representative example is shown for each construct in Figure 4a.

To construct the mCherry–TBA-1 and GFP–DHC-1 constructs, we used standard recombineering techniques with SW102 *E. coli*[38] and Moerman lab fosmids containing the entire promoter, all exons and introns, and the 3′ untranslated regions of *tba-1* and *dhc-1*. Fosmids were obtained from the MRC Geneservice (Cambridge, UK). The mCherry and GFP genes containing *C. elegans* introns[35,39] were inserted at the start codon of the *tba-1* and *dhc-1* genes. We then gap repaired an amplified *Caenorhabditis briggsae unc-119*(+)-containing plasmid[40] such that the entire *tba-1* or *dhc-1* genes (promoters, exons, introns and 3′ untranslated

regions) were captured between the flanking open reading frames. These gap-repaired plasmids were used to transform *unc-119*(–) worms.

Accession numbers. The following sequences used in Figure 4b were obtained from the National Center for Biotechnology Information: *Drosophila melanogaster*: NP_001097874.1, *Acyrthosiphon pisum*: XP_001943684.1, *Nasonia vitripennis*: XP_001603899.1, *Tribolium castaneum*: XP_969387.1, *Pediculus humanus corporis*: XP_002425811.1, *Culex quinquefa*sciatus: XP_001865870.1, *Trichinella spiralis*: ABIR01001549, *Brugia malayi*: XP_001899191.1, *Caenorhabditis elegans*: NP_001122818.1 and *Meloidogyne hapla*: ABLG01000531.1_contig530. Sequences for the following proteins were obtained from the Joint Genome Institute: *Daphnia pulex*: NCBI_GNO_6700040, *Capitella capitata*: scaffold_117:275944-280349, *Lottia gigantea*: fgenesh2_pg.C_sca_5000157. We obtained the CJ976727 EST sequence for *Bursaphelenchus mucronatus* from http://forestgen.ffpri.affrc.go.jp, and the sequence for *Pristionchus pacificus* PPA21096 was obtained from http://wormbase.org.

32. Brenner, S. The genetics of *Caenorhabditis elegans*. *Genetics* **77,** 71–94 (1974).
33. Oegema, K., Desai, A., Rybina, S., Kirkham, M. & Hyman, A. A. Functional analysis of kinetochore assembly in *Caenorhabditis elegans*. *J. Cell Biol.* **153,** 1209–1226 (2001).
34. Strome, S. *et al.* Spindle dynamics and the role of γ-tubulin in early *Caenorhabditis elegans* embryos. *Mol. Biol. Cell* **12,** 1751–1764 (2001).
35. McNally, K., Audhya, A., Oegema, K. & McNally, F. J. Katanin controls mitotic and meiotic spindle length. *J. Cell Biol.* **175,** 881–891 (2006).
36. Praitis, V., Casey, E., Collar, D. & Austin, J. Creation of low-copy integrated transgenic lines in *Caenorhabditis elegans*. *Genetics* **157,** 1217–1226 (2001).
37. Fraser, A. G. *et al.* Functional genomic analysis of *C. elegans* chromosome I by systematic RNA interference. *Nature* **408,** 325–330 (2000).
38. Warming, S., Costantino, N., Court, D. L., Jenkins, N. A. & Copeland, N. G. Simple and highly efficient BAC recombineering using galK selection. *Nucleic Acids Res.* **33**, e36 (2005).
39. Cheeseman, I. M. *et al.* A conserved protein network controls assembly of the outer kinetochore and its ability to sustain tension. *Genes Dev.* **18,** 2255–2268 (2004).
40. Sarov, M. *et al.* A recombineering pipeline for functional genomics applied to *Caenorhabditis elegans*. *Nat. Methods* **3,** 839–844 (2006).

nature cell biology

DOI: 10.1038/ncb2128

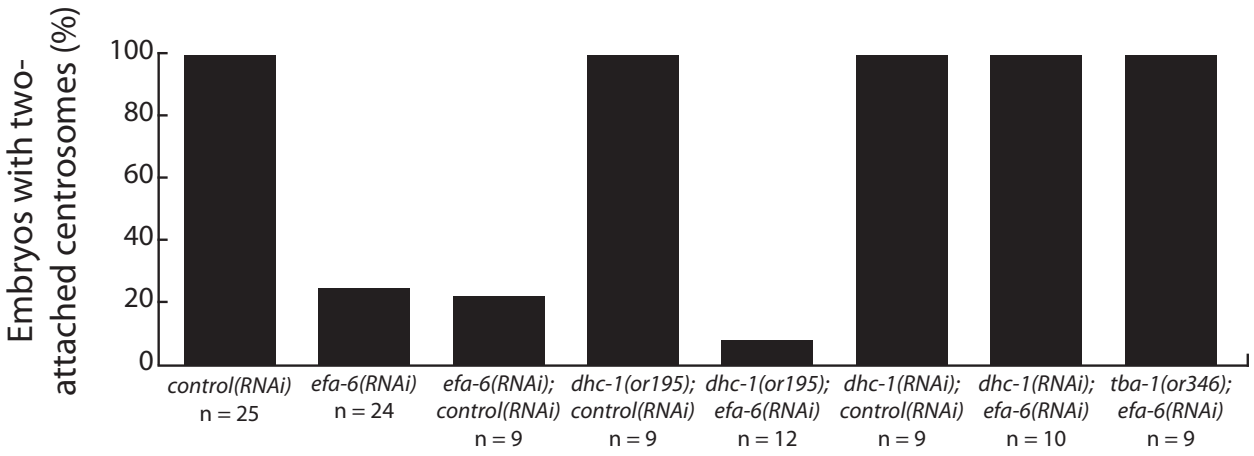

Figure S1 Centrosome detachment in *efa-6(-)* embryos is MT-dependent and dynein-dependent. Summary of the percentage of embryos with both centrosomes attached to the male pronucleus, for each genotype tested (see Fig. 1a for corresponding images and details).

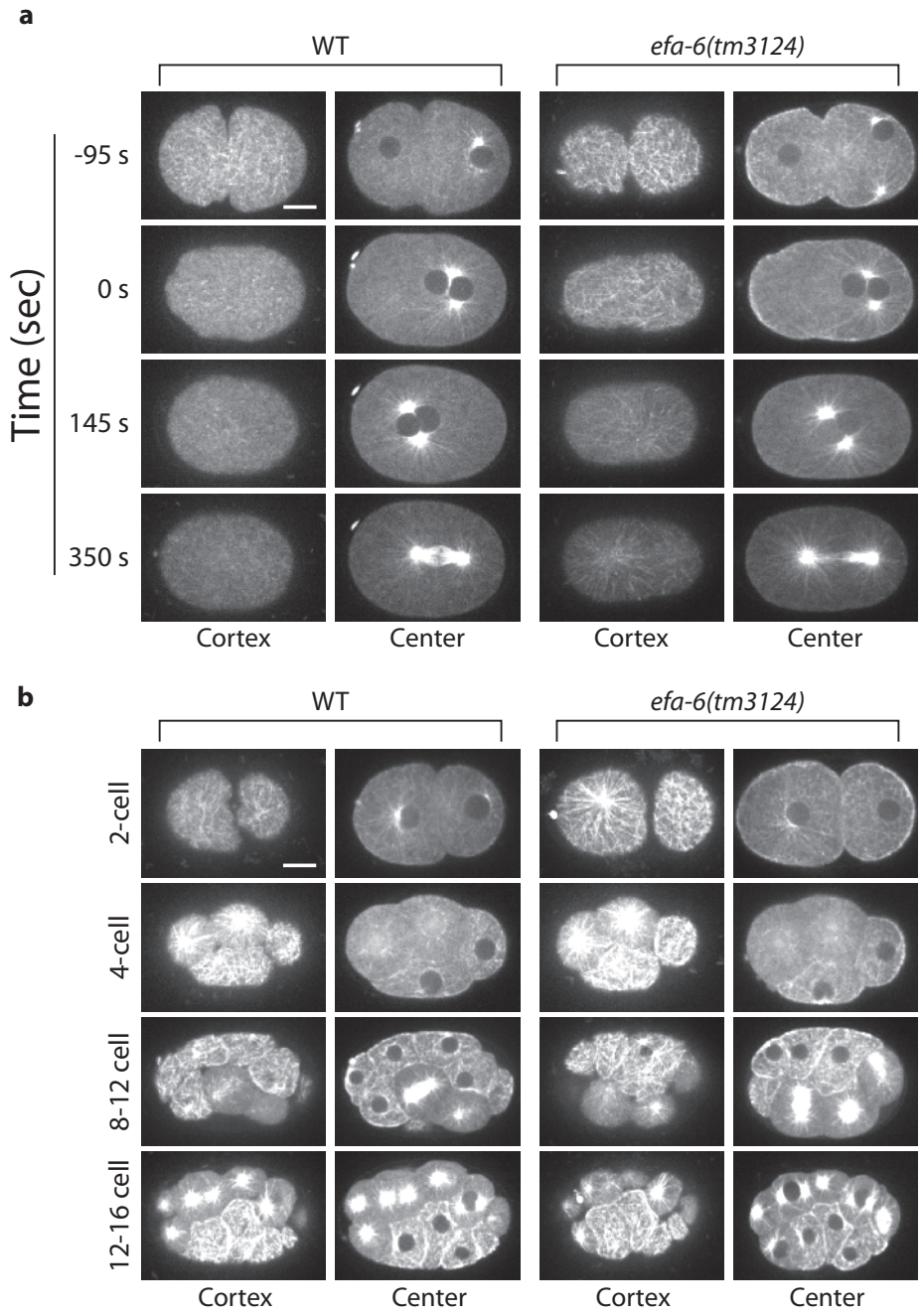

Figure S2 EFA-6 prevents long cortical MTs in one- and two-cell embryos. Wild-type and *efa-6(tm3124)* embryos expressing GFP-β-tubulin. Three Z sections with 0.5 μm spacing were captured and merged to generate the images. **a**, Time-lapse images captured during the first cell cycle, times indicated are relative to pronuclear meeting. Shown for each time point are images captured at the cortical focal plane and the central focal plane. **b**, Images from multicellular embryos. Note that two-cell embryos showed similar cortical MT dynamics as one-cell embryos, but after the four-cell stage both wild-type and *efa-6* mutant embryos displayed abundant cortical MTs. Scale bars, 10 μm.

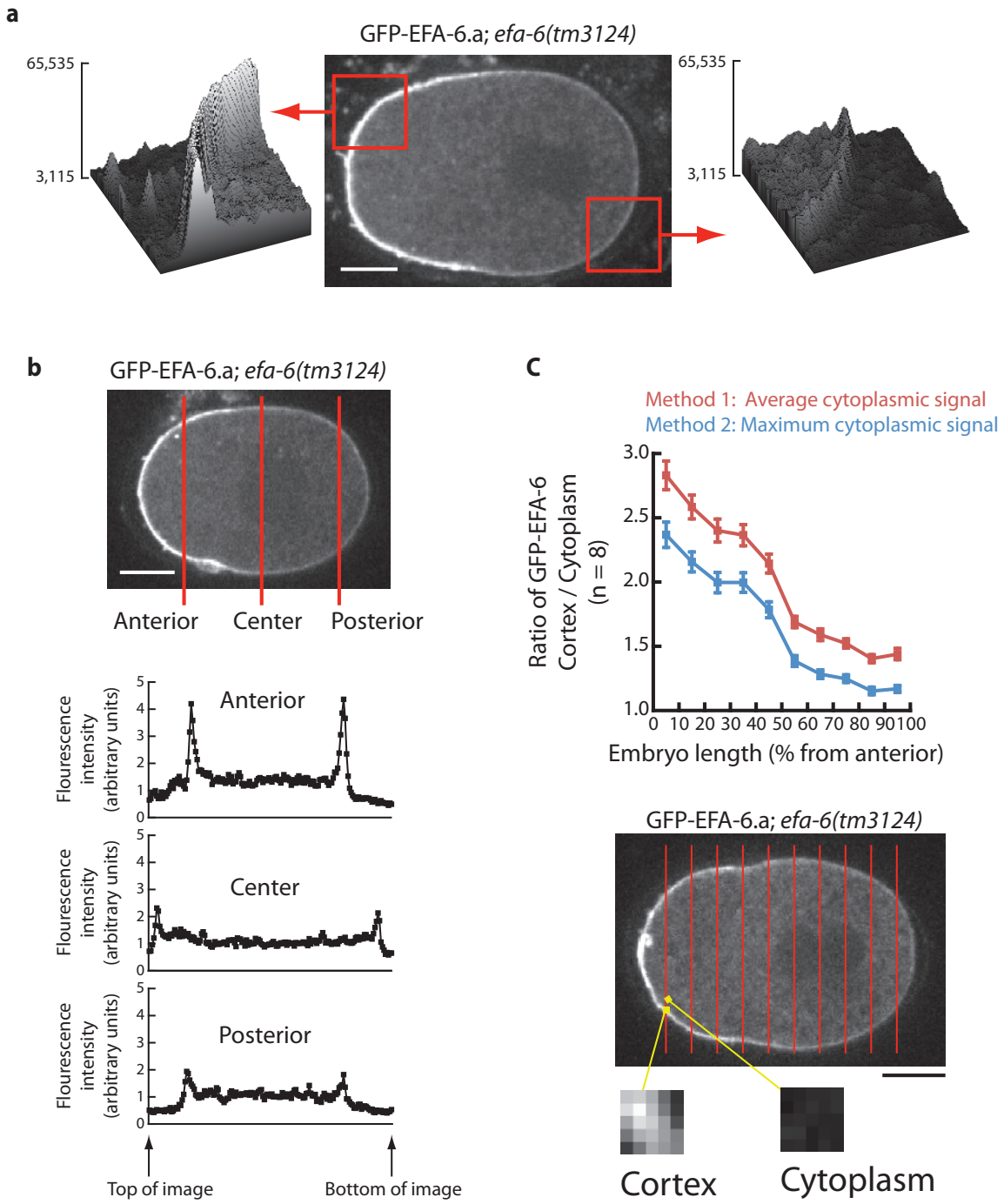

Figure S3 GFP-EFA-6 is present on the cortex. One Z section was obtained for each embryo at a mid-embryonic plane during pronuclear migration. **a**, The indicated regions were analyzed with the "Surface Plot" tool of ImageJ using default parameters. Both the anterior and posterior cortical regions show enrichment for GFP-EFA-6.a. **b**, The three indicated lines were analyzed by the "Plot Profile" tool of ImageJ. Each embryo section shows cortical enrichment for GFP-EFA-6. **c**, Quantitation of the ratio of cortical to cytoplasmic GFP-EFA-6 along the embryo anterior posterior axis. Lines were drawn across embryos (as in Fig. S3b), but ten lines were distributed starting at 5% egg-length and progressing at 10% increments. Where the lines crossed the cortex (at both the top and bottom of each embryo) we obtained the maximum pixel intensity within a 1 μm^2 region. For the cytoplasmic measurement, we obtained both the average pixel intensity (Method 1) and the maximum pixel intensity (Method 2) for a 1 μm^2 region located 1 μm inside the cortical region sampled. We then divided the cortical pixel intensity by the cytoplasmic intensity to generate the plots. Error bars represent the S.E.M. with a confidence interval of 0.95. Eight embryos were examined to generate the plots. The two panels below the embryo have been magnified 10-fold, with respect to the embryo, and denote two positions where we obtained readings. Scale bars, 10 μm.

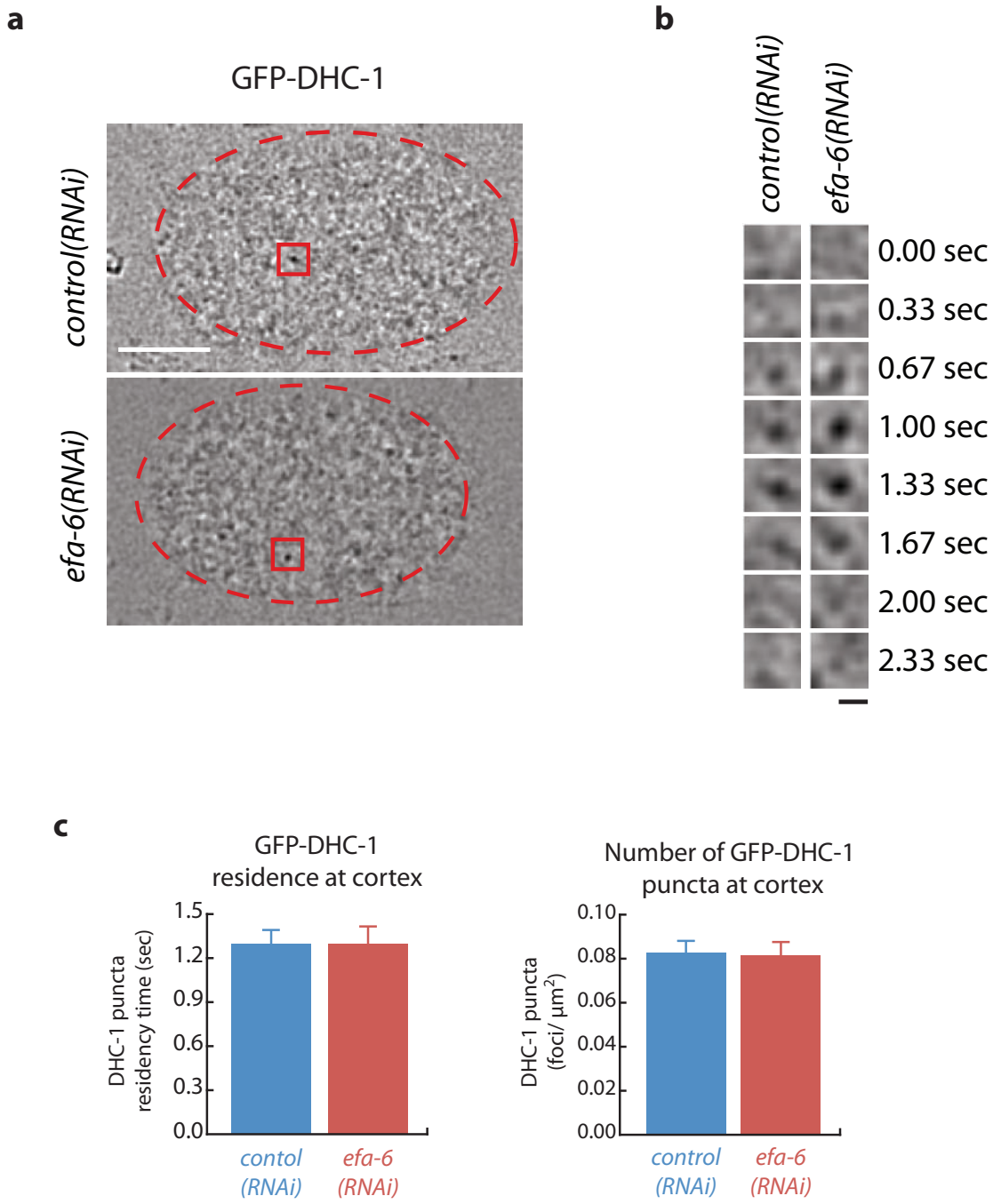

Figure S4 DHC-1 is present at the cell cortex but loss of dynein function does not cause excessive cortical MTs at pronuclear meeting. **a**, GFP-DHC-1 fusion protein at the cortex. To eliminate the ubiquitous diffuse signal we applied a Laplacian filter to the images to detect transient puncta at the cortex. Dashed red ovals indicate the edges of the embryos and the red box indicates a magnified view in presented in panel b. Scale bar, 10 μm. **b**, time-lapse images of the boxed region shown in panel a. Images were captured three times every second and displayed as a montage. Puncta behavior was not different between *control(RNAi)* embryos or *efa-6(RNAi)* embryos. Scale bar, 1 μm. **c**, Quantitation of GFP-DHC-1 puncta residency times and density on the cortex in *control(RNAi)* and *efa-6(RNAi)* embryos. Error bars represent the S.E.M. with a confidence interval of 0.95.

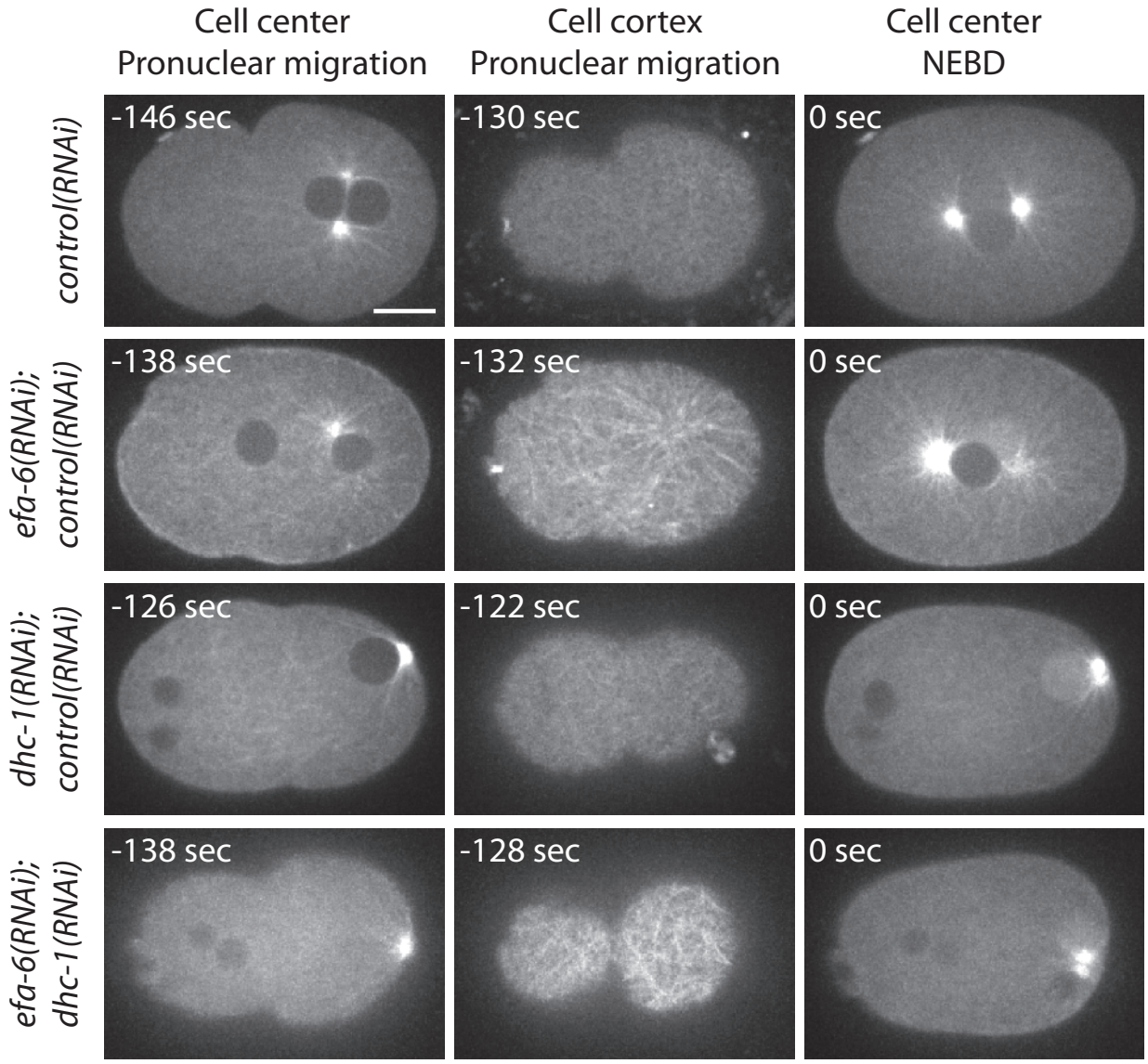

Figure S5 Embryos simultaneously depleted for both *efa-6* and *dhc-1* exhibit dense cortical MTs during pronuclear migration. mC-TBA-1-expressing embryos were examined for MT distribution at the indicated times and focal planes. The *control(RNAi)* and *dhc-1(RNAi)* embryos exhibited few MTs at the cortex but the *efa-6(RNAi); control(RNAi)* and *efa-6(RNAi); dhc-1(RNAi)* embryos displayed robust MTs at the cortex. The *dhc-1*-depleted embryos display un-separated centrosomes, multiple maternal pronuclei due to polar body extrusion defects, and centrosomes that remained attached to the male pronucleus, indicating a severe loss of dynein activity. Three Z sections with 0.5 μm spacing were captured and merged to generate the images, times (in seconds) are relative to nuclear envelope breakdown. Scale bar, 10 μm.

Supplementary movie legends

Movie S1 *Control(RNAi)* and *efa-6(RNAi)* embryos expressing GFP-γ-tubulin and GFP-histone were imaged at 7 focal planes 1.5 μm apart every 4 sec, The focal planes were subsequently merged. Embryos are at the pronuclear migration stage, anterior to the left. Playback is 10 frames/ sec (fps).

Movie S2 *dhc-1(or195)*; *control(RNAi)* and *dhc-1(or195)*; *efa-6(RNAi)* embryos expressing GFP-γ-tubulin and GFP-histone were imaged at 11 focal planes 1 μm apart every 4 sec and the planes were merged. Embryos were imaged 30- 90 min after shifting worms from 15 °C to 26 °C. The video starts prior to pronuclear meeting, anterior to the left. Playback is 8 fps.

Movie S3 *dhc-1(RNAi); control(RNAi)* and *dhc-1(RNAi)*; *efa-6(RNAi)* embryos expressing GFP-γ-tubulin and GFP-histone were imaged at 11 focal planes 1.5 μm apart every 10 sec and the planes were merged. Embryos were examined 27-37 hours after L4 hermaphrodites were transferred to *E. coli* expressing the double-stranded RNAs. The video starts when centrosome separation would normally occur and ends at pronuclear envelope breakdown, anterior to the left. Playback is 7 fps.

Movie S4 *Control(RNAi)* and *efa-6(RNAi)* embryos expressing GFP-γ-tubulin and GFP-histone were imaged at 3 focal planes 1 μm apart every 2 sec at the cell center and the planes were merged. The video starts at the metaphase to anaphase transition, anterior to the left. Playback is 30 fps.

Movie S5 Wild-type and *efa-6(tm3124)* embryos expressing GFP-β-tubulin were imaged at three focal planes 0.5 μm apart every 5 sec (at both the cortical plane, left, and at the spindle plane, right) and the slices were merged to give cortical and spindle views. The video starts at pronuclear migration, anterior to the left. Playback is 15 fps.

Movie S6 Wild-type and *efa-6(tm3124)* embryos expressing EBP-2-GFP and mCherry-histone were imaged at one focal plane every 1 sec. The video starts during pronuclear migration viewing the central focal plane of the embryo, anterior to the left. At 6 sec, the focus is adjusted to view the cortical plane. The top portion of the video displays single images and the lower portion displays five consecutive time points merged. Playback is 10 fps.

Movie S7 A wild-type embryo expressing GFP-DHC-1 was imaged at the cortex at a rate of 3 frames/ sec beginning at pronuclear meeting. The left side shows the fluorescent image and the right side shows the Laplacian filtered image. Playback rate is 15 fps.